

PACS numbers: 42.25.Dd; 42.25.Fx; 42.25.Kb; 02.70.Uu
DOI: 10.1070/QE2014v044n01ABEH015292

Low-coherence interferometry as a method for assessing the transport parameters in randomly inhomogeneous media

D.A. Zimnyakov, J.S. Sina, S.A. Yuvchenko, E.A. Isaeva, S.P. Chekmasov, O.V. Ushakova

Abstract. **The specific features of using low-coherence interferometric probing of layers in randomly inhomogeneous media for determination of the radiation propagation transport length both in diffuse regime and in the case of optically thin media are discussed. The transport length is determined by the rate of exponential decay of the interference signal with the increase in the path length difference between the light beams in the reference arm of the low-coherence interferometer and in the object arm, containing the probed layer as a diffuse reflector. The results are presented of experimental testing of the discussed approach with the use of layers of densely packed titanium dioxide nanoparticles and polytetrafluoroethylene.**

Keywords: *scattering, low-coherence interferometry, disperse systems, transport length, diffusion approximation, Monte Carlo modelling.*

1. Introduction

During the last three decades the optical properties of micro- and nanostructured disperse media have been a subject of intense studies. This is caused by the prospects of creating new materials with unique characteristics in the UV, visible, and IR ranges on their basis. For media with a regular structure such uniqueness manifests itself in the existence of photonic band gaps [1–3], on the basis of which, in combination with nonlinear-optical properties of the medium structure components, one can implement principally new optical elements (e.g., selective filters, convertors of sub-picosecond laser pulses, etc [4, 5]). The synthesis of structurally ordered media, characterised by nonmonotonic frequency dependences of effective values of permittivity and permeability and their negative values within certain frequency intervals, provides the background for fabricating so called left-handed media (metamaterials) in the optical range [6–8].

The interest in the optical properties of randomly inhomogeneous disperse materials is caused by the prospects of their applications as high-efficiency radiation convertors in photoelectric devices [9], as the basis for creating laser media with disordered structure [10, 11], and the materials for photobilological applications [12].

D.A. Zimnyakov Saratov State Technical University, ul. Politekhnicheskaya 77, 410054 Saratov, Russia; Institute of Precise Mechanics and Control, Russian Academy of Sciences, ul. Rabochaya 24, 410024 Saratov, Russia: e-mail: zimnykov@mail.ru;
J.S. Sina, S.A. Yuvchenko, E.A. Isaeva, S.P. Chekmasov, O.V. Ushakova Saratov State Technical University, ul. Politekhnicheskaya 77, 410054 Saratov, Russia

Received 31 July 2013; revision received 6 October 2013
Kvantovaya Elektronika **44** (1) 59–64 (2014)
Translated by V.L. Derbov

The optical radiative transfer in weakly absorbing isotropic randomly inhomogeneous media is determined by the following transport parameters of the medium:

– the transport length of radiation propagation l^* in the medium, determined by the characteristic spatial scale of the conversion of the directed radiation component into the diffuse component [13];

– the scattering length $l \leqslant l^*$ (the mean distance of propagation of the scattered field partial components between the scattering events) [13];

– the effective refractive index n_{eff} [14] that determines the phase velocity of the partial components in the medium and, correspondingly, the coefficients of reflection of the partial components from the boundary between the medium and the free space.

In turn, the quantities l^*, l, and n_{eff} are determined by the radiation wavelength λ, the volume fraction of the scattering centres f in the medium, the mean size $\bar{r}$ and the refractive indices of the scatterers n_c and the matrix medium between the scatterers n_f (for weakly absorbing media the imaginary parts of n_c and n_f may be assumed zero). The transport parameters of the medium characterise its properties as disperse optical material and, therefore, the problem of their determination is one of the key problems in the synthesis of such systems with prescribed optical characteristics. One of the most popular methods of assessing l^* and l is to measure the diffuse (T_d) and collimated (T_c) transmittance of a medium layer, as well as its diffuse reflection R_d, and then to calculate the scattering coefficient $\mu_s = 1/l$ and the transport scattering coefficient $\mu_s' = 1/l^*$ by using the measurement data. For this aim various approaches to approximate solution of the inverse radiative transfer problem in the layer can be applied (adding-doubling method, inverse Monte Carlo method, etc. [15–17]). A simple and elegant method for determining l^* with the use of a laser beam, obliquely incident on the medium, was proposed by L.Wang, and S.Jacques [18]. In Refs [19, 20] a speckle-correlation method of transport length assessment in randomly inhomogeneous media is discussed. The method is based on the binary frequency modulation of the probing laser radiation and the analysis of speckle-structure decorrelation in the scattered radiation depending on the modulation frequency shift. In Ref. [21] and alternate approach to the assessment of l^* in unsteady randomly inhomogeneous media using a localised coherent radiation source and spatial filtering of a speckle-modulated image of the probed object surface by means of ring filters having different radii is considered.

It is necessary to note that in the measurements of l^*, using both the Wang–Jacques method and the above speckle-correlation methods, the obtained results also depend on n_{eff}, which leads to the necessity of exploiting independent techniques to determine this parameter. A similar problem arises,

e.g., in frequency modulation methods [22, 23] used to determine μ_s and μ'_s.

To assess n_{eff}, a method was proposed [24] based on the analysis of polarisation-dependent angular distributions of light intensity, diffusely scattered by the medium. The method yields the values of n_{eff} that agree with the initial data about the structure and dielectric properties of the studied materials. However, it is worth mentioning a certain complexity of the instrumental implementation of this method, as well as high labour consumption of measurements and interpretation of the obtained results.

In the present paper we consider a method for assessing the transport parameters in randomly inhomogeneous media on the basis of interferometric probing of a medium layer with the thickness L, used as a diffuse reflector in the object arm of the interferometer with the low-coherence radiation source. It is shown that, in contrast to the abovementioned methods, the assessment of l^* and n_{eff} from the dependence of the interference signal on the beam path length difference z between the reference and the object arms of the interferometer can be obtained without any additional independent measurements both in optically thick samples with $L \gg l^*$ and for $L \ll l^*$. In the latter case the exponential decay of the interference signal at large z is due to the existence of the radiation components in the thin layer that propagate along the layer by the distance strongly exceeding both L and l^* (spatially confined diffusion of radiation). To interpret the obtained data two approaches are used, one of them based on the effective medium model at $L \gg l^*$ and the other using statistical modelling of radiative transfer in optically thin layers.

2. Experimental technique and experimental data

At present the interferometric method for analysing layered media by means of partially coherent radiation is widely used in biology and medicine to visualise the structure of near-surface biotissue layers (optical coherence tomography, [25–28]), as well as in metrology and material science (see, e.g., [29, 30]). The layered object under study plays the role of a reflector in the object arm of a double-beam interferometer (the Michelson scheme is commonly used), while the optical path length of the reference beam is periodically varied (e.g., as a result of longitudinal back-and-forth motion of the reflector in the reference arm of the interferometer). In the case of using a source of partially coherent radiation the depth of interference modulation of the output beam intensity is maximal when the optical propagation path length of the reference beam coincides with that of the object beam, reflected from the boundary between the adjacent layers (i.e., when the optical path difference is zero). With the growth of the path difference absolute value as a result of motion of the reflector in the reference arm, the depth of the interference modulation decreases to zero, and in the case of path difference exceeding the source coherence length the output signal of the interferometer is equal to the sum of intensities of incoherent object and reference beams. When probing a transparent object having a layered structure, the output signal of the interferometer is a sequence of interference 'packets' with the position in the time scan of the signal determined by the depth of occurrence of the corresponding layers in the object, and the envelope determined by the shape of the coherence function of the used radiation source. The maximal depth of interference modulation for each packet is determined by the amplitude coefficient of reflection of the probe radiation from the corresponding boundary between the adjacent layers, i.e., by the ratio of refractive indices of the layers. The analysis of the interference signal time scan allows obtaining the data on the position and values of relative refractive indices of the layers in the object.

Note that in the case of traditional analysis of partially transparent layered media the stochastic component of the recorded signal caused by the diffuse scattering of the probing radiation from the medium volume into the object arm of the interferometer is a negative factor that reduces the limit of possible depth of medium probing and leads to parasitic speckle-modulation of the signal. On the contrary, in the cases of low-coherence interference probing of multiply scattering media, considered in the present paper, just the dependence of the dominant contribution of diffusely scattered components into the interference signal on the probing depth is analysed.

The experiments on low-coherence probing of layers in randomly inhomogeneous media were carried out using the Thorlabs OCS1300SS optical coherence tomograph (the centre wavelength 1325 nm, the coherence length in air 6 mm). The studied samples were the 100-μm-thick FUM fluoroplastic tape, for which the expected value of the transport length is comparable with the sample thickness, and the layers of polydisperse particles of titanium dioxide with the mean size no greater than 25 nm (TiO_2 nanopowder for preparing the layers Aldrich 637254, Sigma-Aldrich, USA) between glass substrates (the substrate thickness was 1.0 mm, the layer thickness was regulated by spacers and amounted to 200–250 μm). The volumetric tests of the nanopowder have shown that its apparent density equals 0.293 ± 0.05 g cm^{-3}. The passport values of the apparent density for the Aldrich 637254 product are essentially lower and amount to 0.04–0.06 g cm^{-3}, which allows the assumption that the source material contains a significant amount of nanoparticle aggregates, whose mean size exceeds 25 nm. By estimate, the initial value of f is 0.075, and after compressing the layers between the substrates $f \approx 0.23$.

Figure 1 presents the amplitude of the interference signal versus the path length difference z for the beams in the reference and the object arm (the z values are presented for free

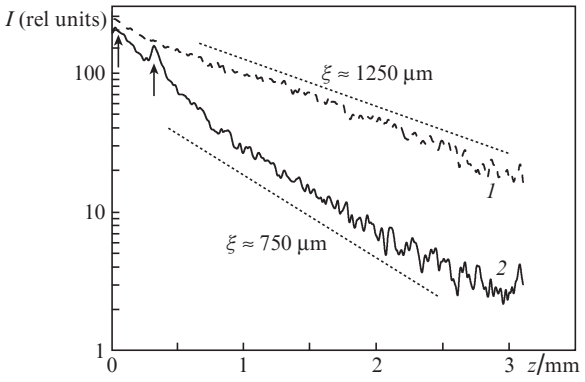

Figure 1. Dependences of the low-coherence interferometer output signal on the geometric path length difference of the beams in reference and object arms with the probed ~230-μm-thick layers of TiO_2 particles and the FUM tape used as diffuse reflectors in the object arm (the arrows point at the peaks of Fresnel reflection from the upper and lower boundaries of the tape). Dotted lines show the dependences $I(z) \sim \exp(-z/\xi)$.

space without taking the probed medium refractive index n_{eff} into account). The specific feature of the presented dependences is the exponential decay of the intensity with the growth of z [$I(z) \backsim \exp(-z/\xi)$] that takes place at path length differences, for which the signal-to-noise ratio is greater than one. For the studied samples the intervals of exponential decay of the signal span over 1.5 decades. The other peculiarity of the dependence in FUM samples is the peak, caused by Fresnel reflection of the probing beam from the lower boundary of the layer (the maxima of the signal, caused by the reflections from the boundaries, are pointed with arrows). For the layers of TiO_2 nanoparticles this peak is not observed, since $L \gg l^*$. According to the estimates, $\xi = 750 \pm 30$ μm for the FUM samples and 1250 ± 50 μm for the layers of titanium dioxide nanoparticles.

3. Discussion of the experimental results

3.1. Low-coherence interferometric probing of randomly inhomogeneous media in the regime $L \gg l^*$

There is an analogy between the time-domain medium response in the regime of detecting the backscattered radiation when probing the medium with a short light pulse and the interference signal, recorded in the low-coherence interferometer with the probed medium in the object arm [31]. For the technique used in the present paper, the low-coherence probing with the source coherence length 6 mm is equivalent to the pulsed-modulation probing with the pulse duration $\sim 2 \times 10^{-11}$ s. In the diffusion approximation [13] the temporal response of the optically thick medium layer in the regime of detecting the backscattered radiation is described by the expression [31]:

$$R_{\text{d}}(t) = \frac{3D}{l^* \tilde{L}} \exp\left(-\frac{t}{\tau_{\text{a}}}\right) \times \times \sum_{n=1}^{\infty} \left\{ \exp\left(-\frac{D\pi^2 n^2}{\tilde{L}^2} t\right) \left[1 - \cos\left(\frac{l^* + Z_1}{\tilde{L}} 2\pi n\right)\right]\right\}. \quad (1)$$

Here $D = l^* v_E/3$ is the radiation diffusion coefficient; v_E is the radiation energy transfer velocity in the medium; τ_{a} is the characteristic time of absorption (for weakly absorbing media $\tau_{\text{a}} \to \infty$); $\tilde{L} = L + l^*(Z_1 + Z_2)$;

$$Z_{1,2} = \frac{2 + \int_0^1 4\mu R_{1,2}(\mu)\,\mathrm{d}\mu}{3 - \int_0^1 9\mu^2 R_{1,2}(\mu)\,\mathrm{d}\mu} \quad (2)$$

are dimensionless coefficients, determined by the reflective ability of the layer boundaries [32]; $\mu = \cos\theta$; θ is counted from the normal to the surface inside the layer; and $R_{1,2}(\mu)$ are equal to Fresnel reflection coefficients of the boundaries for unpolarised light, the incidence angle being equal to θ.

For $\tau_{\text{a}} = \infty$ and $t > \tilde{L}^2/(\pi^2 D)$ the asymptotic behaviour of $R_{\text{d}}(t)$ is described by the exponential function $R_{\text{d}}(t) \sim \exp(-t/\tau_{\text{d}})$ with τ_{d} defined by the expression

$$\tau_{\text{d}} \approx \frac{3\tilde{L}^2}{\pi^2 l^* v_E}. \quad (3)$$

In the case of low-coherence probing in media with small material and structural dispersion, the time of light pulse propagation in the medium is related to the path length difference of the beams in the interferometer as $z = v_E t \approx ct/n_{\text{eff}}$. Hence, in the diffusion approximation

$$\xi \approx \frac{3}{\pi^2} \frac{n_{\text{eff}} \{L + l^*[Z_1(n_{\text{eff}}) + Z_2(n_{\text{eff}})]\}^2}{l^*}. \quad (4)$$

Analysing the case of probing optically thick layers of TiO_2 nanoparticles (Fig. 1) we see that the same values of ξ can be obtained with different combinations of the parameters l^* and $Z_1(n_{\text{eff}}) = Z_2(n_{\text{eff}}) = Z(n_{\text{eff}})$. In other words, to each value of ξ measured in the experiment corresponds a curve $l^* = \varphi(n_{\text{eff}})$ in the coordinate plane (n_{eff}, l^*). On the other hand, for given λ and f different values of l^* and n_{eff} correspond to different values of the mean size of the particles in the layer. Such a relation is also described by a certain curve $l^* = \psi(n_{\text{eff}})$. The crossing point of the curves $l^* = \varphi(n_{\text{eff}})$ and $l^* = \psi(n_{\text{eff}})$ allows the determination of the parameters n_{eff} and l^*, characterising the probed medium.

One of the possible ways to determine l^* and n_{eff} for given λ, f, and $\langle r \rangle$, as well as the refractive index of the particles and the base medium, is to apply the effective medium model. When this approach is used to find the transport parameters of randomly inhomogeneous media with a large volume fraction of scattering centres, merged in non-absorbing matrix medium and consisting of non-absorbing material, one should consider a model spatially homogeneous medium with the complex dielectric constant $\varepsilon = \varepsilon' + i\varepsilon''$. The unknown parameters ε' and ε'' of the effective medium are determined from the condition of equality between the decay coefficients for the propagation of a plane electromagnetic wave in the real medium and in the model one. To check this condition a certain volume of the effective medium is replaced with the equivalent volume of the modelled scattering medium (trial scattering centre), which consists of a randomly chosen scattering particle enclosed in the shell of a matrix medium. For isotropic randomly inhomogeneous media, consisting of spherical and spheroidal particles, the trial scattering centre is chosen in the form of a spherical core of the scatterer material coated with a spherical shell of the matrix medium. The radius of the spherical core and the shell thickness are chosen using the data on the size of the scatterers and their volume fraction in the modelled medium [33]. The immersion of the trial scattering centre into the effective medium should not change the conditions for the electromagnetic field propagation in comparison with the field propagation in the spatially homogeneous effective medium. In order to attain this condition, various approaches may be applied, in particular, the approach on the basis of minimisation of the forward scattering amplitude $A(0)$ [13, 14] for the trial scattering centre [34]. The value of $A(0)$ for the given core radius and shell thickness of the trial scatterer, as well as the dielectric constants of the core, the shell, and the effective medium are calculated by means of the known algorithm for solving the problem of electromagnetic wave scattering from a sphere coated with a shell (see, e.g., [14]). Using the recurrence procedure, the parameters ε', ε'' of the effective medium are varied until the value of $A(0)$ nearest to zero is achieved. For polydisperse scattering systems the criterion of minimising the value of $\langle |A(0)| \rangle$ averaged over all possible scatterer sizes is used.

In searching for ε', ε'' of the effective medium, the complex wavenumber $\tilde{k} = k' + i/2l$ for the radiation, propagating through the medium, is determined [33], which satisfies the criterion of minimal $\langle |A(0)| \rangle$. The effective refractive index of the modelled medium is expressed as $n_{\text{eff}} = \mathrm{Re}\,\tilde{k}/k_0$ (k_0 being the wavenumber of the probing radiation in free space), and the scattering length is expressed as $l = 1/(2\mathrm{Im}\,\tilde{k})$. Then, using the found values of n_{eff} and l, the transport length l^* is deter-

mined. For this purpose the recursive procedure of minimising the difference $\langle\sigma_t\rangle - \langle\sigma_{as}\rangle$ [34] is used, where $\langle\sigma_t\rangle$ and $\langle\sigma_{as}\rangle$ are the extinction cross section and the asymmetry parameter, respectively, [14] for the trial scattering centre, obtained as a result of averaging over all possible sizes of the scattering particles. In particular, this approach was successfully applied to the interpretation of the results of measuring T_d and the angular width of the peaks of coherent backscattering for the media based on densely packed TiO_2 particles [35].

Figure 2 presents the dependence $l^* = \varphi(n_{eff})$, corresponding to the value $\xi \approx 1250$ μm obtained in the experiment for the layer of TiO_2 particles with the thickness 230 ± 5 μm, and the dependence $l^* = \psi(n_{eff})$ for the model system of spherical particles with different values of the radius $\langle r\rangle$ and fixed f = 0.23. The dependence $l^* = \psi(n_{eff})$ was found using the effective medium model described above; the refractive index of the scatterers for λ = 1325 nm was taken to be ~2.75 in correspondence with Ref. [36]. The crossing point for the curves $l^* = \varphi(n_{eff})$ and $l^* = \psi(n_{eff})$ yields $l^* \approx 21.2 \pm 1.3$ μm and $n_{eff} \approx 1.283 \pm 0.002$. The corresponding value of $\langle r\rangle$ amounts to 85–90 nm, which allows the conclusion about the dominant contribution of nanoparticle aggregates into the scattering. In the low-frequency limit $\langle r\rangle/\lambda \to 0$ the values, calculated using the effective medium model, asymptotically tend to the value, resulting from the Maxwell–Garnett model [14] for the probed disperse medium ($n_{eff} \approx 1.250$, marked by a vertical dotted line in Fig. 2), remaining to be slightly greater than it.

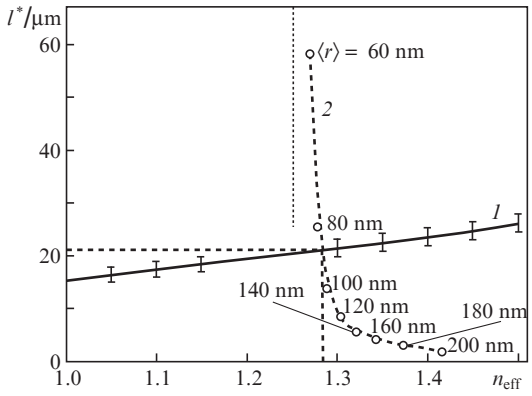

Figure 2. Dependence $l^* = \varphi(n_{eff})$ (*1*), obtained for $\xi \approx 1250$ μm (the layer of TiO_2 particles, Fig. 1) using Eqn (4), and the dependence $l^* = \psi(n_{eff})$ (*2*), obtained using the effective medium model by minimising the amplitude of forward scattering for the trial scattering centre having the form of a spherical particle coated with a shell. The vertical dotted line corresponds to the value of n_{eff} that follows from the Maxwell–Garnett model in the low-frequency limit. The points at curve (*2*) are the result of calculations with different values of $\langle r\rangle$.

The measurements of l^* for λ = 1325 nm using other methods were not carried out; however, the obtained value can be compared with the data on diffuse transmittance T_d and reflection R_d from the layers of Aldrich 637254 nanopowder with a similar f value in the interval of wavelengths 450–1050 nm. The measurements were carried out using the Ocean Optics QE65000 spectrometer and the Thorlabs IS236A-4 integrating sphere; the values of l^* and n_{eff} were determined using the inverse Monte Carlo method. In correspondence with the obtained data, the quantity l^* for this disperse system monotonically grows from ~8.9 μm at λ = 450 nm to ~17.1 μm at λ = 1050 nm. Such a significant growth of l^* with increasing λ is caused by strong dependence of the scattering efficiency factor for the particles with $\langle r\rangle < \lambda$ on their diffraction parameter $2\pi\langle r\rangle n_b/\lambda$, where n_b is the refractive index of the medium, containing the particles. Keeping in mind this tendency in the behaviour of l^*, one can conclude that the value, obtained for λ = 1325 nm, satisfactorily agrees with the result of measuring T_d and R_d at smaller wavelengths.

3.2. Low-coherence interferometric probing of randomly inhomogeneous media in the regime $L \leqslant l^*$

For layers with $L \leqslant l^*$ the diffusion approximation of the radiative transfer theory [Eqns (1), (3), (4)] is not valid. Nevertheless, the results of statistical modelling of radiative transfer show that the exponential decay of the signal 'tail' in the regime of backscattering with the growth of t (in pulsed-modulation probing) or z (in low-coherence interferometry) also takes place in this case. Figure 3 presents the probability density functions for the values s of the path length of partial components, obtained at different values of l^*/L. The used Monte Carlo modelling procedure is similar to that described in Refs [37, 38]. The scattering phase function was accepted to have the Henyey–Greenstein form that provides an adequate description of a 'single-particle' scattering indicatrix for various randomly inhomogeneous media within a wide range of the scattering anisotropy parameter values [39]. The high-amplitude peaks of $\rho(s)$ near $s = 2L$ at $l^*/L > 1$ correspond to the Fresnel reflection of the probing beam from the lower boundary of the layer (the peaks from the upper boundary are not shown in the Figure). The presented distributions demonstrate exponential decay of $\rho(s)$ in the region of large s. Note that the distributions $\rho(s)$ at l^*/L = 0.1 and 2 are characterised by nearly the same decay rate of the exponential tail, but correspond to different branches (ascending and descending) of the dependence of ξ on l^* (Fig. 4).

The presence of Fresnel reflection peaks in the dependence $I(z)$ for the FUM sample (see Fig. 1) with the known layer thickness 100 μm allowed the determination of its effective refractive index $n_{eff} \approx 1.45$ that was then used in the modelling. Thus, similar to the case $L \gg l^*$, in the case $L \leqslant \xi$ at

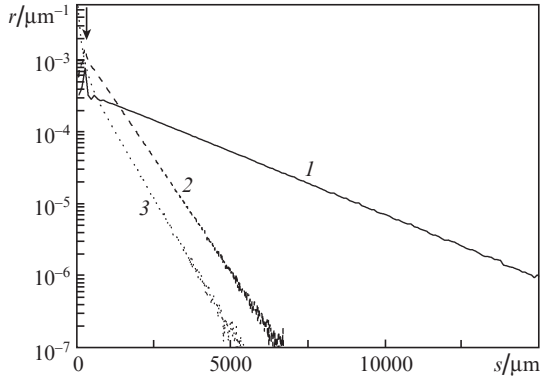

Figure 3. Probability density functions for the path lengths of partial components of the field, scattered in randomly inhomogeneous layer in the processes of probing with a short light pulse and detecting the back-scattered radiation (Monte Carlo modelling) at l^*/L = (*1*) 10, (*2*) 2 and (*3*) 0.1. The arrow points at the peaks of Fresnel reflection from the lower boundary of the layer (the peaks from the upper boundary are not shown).

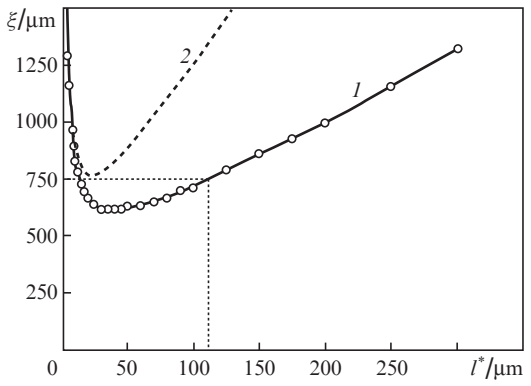

Figure 4. Dependences of ξ on l^* for the layer with the thickness 100 μm with $n_{\text{eff}} = 1.45$; (*1*) Monte Carlo modelling; (*2*) diffusion approximation [Eqn (4)].

large z the signal decreases following the exponential law $I(z) \backsim \exp(-z/\xi)$. Figure 4 presents the dependence of ξ on l^* for the layer with the thickness 100 μm and $n_{\text{eff}} = 1.45$, obtained from the data of Monte Carlo modelling. In the same figure the dependence, corresponding to the diffusion approximation [Eqn (4)] is presented. The quantity $Z_1 = Z_2 = Z$ for the layer–air boundaries was calculated using Eqn (2); the value of Z amounted to ~2.11. The discrepancy between the value of ξ, corresponding to the numerical solution of the transport equation (Monte Carlo modelling), and the overestimated value, given by the diffusion approximation, becomes unacceptable (greater than 10%) at $l^*/L > 0.25$. Using the experimentally determined $\xi \approx 750$ μm for the FUM sample, the model dependence $\xi = \varphi(l^*/L)$ allows the assessment of l^* as 115 ± 7 μm (the unacceptably small value $l^* \approx 14$ μm, corresponding to the descending branch of the dependence, was neglected). This is in good agreement with the ratio of Fresnel reflection peak amplitudes from the upper and lower boundaries of the layer (~0.19 with the contribution of diffuse components of the signal taken into account, see Fig. 1). Assuming the character of scattering in the layer to be near-isotropic (which is to be valid in the near-IR region), $l^* \approx l$, and the peak ratio is to be $\exp(-2L/l^*) \approx 0.18$.

Now we proceed to considering the peculiarities of propagation of the scattered field partial components with $s \gg l^*$ in the layers with $L \ll l^*$. The exponentially decaying 'tail' of the signal in the case $L \ll l^*$ is due to the diffusion of partial components with s, essentially exceeding l^*, along the layer. Let us estimate the influence of l^* and n_{eff} on ξ in the regime of isotropic scattering, when $l^* \approx l$. Considering an arbitrarily chosen partial component of the scattered radiation, propagating along the layer, let us determine the relevant fraction of the energy flux, remaining in the layer after each scattering event. For the isotropic phase function $p(\theta,\phi) = 1/4\pi$ only those components of the angular spectrum of the scattered partial component will stay in the layer, for which the directions of propagation form the angle with the normal to the layer surface exceeding the critical angle $\theta' = \arcsin(1/n_{\text{eff}})$. For each scattering event one can write the approximate relation between the partial component energy fluxes before and after the Nth scattering event

$$W_{N+1} \approx \frac{\int_{-\theta'}^{\theta'}\int_0^{2\pi} p(\theta,\phi)\sin\theta\,\mathrm{d}\theta\mathrm{d}\phi}{\int_{-\pi/2}^{\pi/2}\int_0^{2\pi} p(\theta,\phi)\sin\theta\,\mathrm{d}\theta\mathrm{d}\phi} W_N = \frac{\sqrt{n_{\text{eff}}^2 - 1}}{n_{\text{eff}}} W_N.$$

For a large number of scattering events

$$W_N \sim \exp\left[-N\ln\left(\frac{n_{\text{eff}}}{\sqrt{n_{\text{eff}}^2 - 1}}\right)\right] \approx \exp\left[-\frac{z}{l^*}\ln\left(\frac{n_{\text{eff}}}{\sqrt{n_{\text{eff}}^2 - 1}}\right)\right], \quad (5)$$

where z is the distance, passed by the partial component in the layer. This model predicts exponential decay of the signal, generated by the partial components with $s \gg l^*$ propagating along the layer. In the isotropic scattering regime

$$\frac{\xi}{n_{\text{eff}}} = \left[\ln\left(\frac{n_{\text{eff}}}{\sqrt{n_{\text{eff}}^2 - 1}}\right)\right]^{-1} l^*.$$

By means of Monte Carlo modelling the values of ξ/n_{eff} were obtained for the layers with $L/l^* = 0.02$ at different values of the scattering anisotropy parameter $g = 1 - l/l^*$ and n_{eff}. The results of the modelling are presented in Fig. 5 as dependences of $K = \xi/l^* n_{\text{eff}}$ on

$$\Gamma = \left[\ln\left(\frac{n_{\text{eff}}}{\sqrt{n_{\text{eff}}^2 - 1}}\right)\right]^{-1}.$$

In the near-isotropic scattering regime ($g = 0.1$) $\xi/l^* n_{\text{eff}} \cong \Gamma$. With increasing scattering anisotropy the values of K decrease, in spite of predominant scattering into the volume of the layer at $g \to 1$. This is due to the growth of the number of scattering events N along the distance $\sim l^*$; the value of N can be estimated as $1/(1-g)$. In the case of strong scattering anisotropy ($g \geqslant 0.85$–0.90) and $n_{\text{eff}} > 22$ the value of K is virtually unchanged with the growth of the effective refractive index of the layer. Note that the dependence of ξ on l^*, as well as the influence of n_{eff} and g on K in the case of broad-band sources should lead to spectral selection of radiation, propagating along the layer in the regime of spatially confined diffusion. For the layers, consisting of Rayleigh particles ($\tilde{a} \ll \lambda$, $\tilde{a}$ being the particle size) a trivial shift of the spectrum of diffuse components with $s \gg l^*$ towards the long-wavelength region should be observed. At the same time, for layers consisting of lager particles ($\tilde{a} \sim \lambda$) the increase in l^* will be accompanied by the essential growth of the scattering anisotropy parameter, which should lead to a faster decay of long-wavelength components. A definite effect is expected also from the peculiarities of the medium dispersion characteristic that lead to variations of n_{eff} with changing λ. Note that because of small intensities of the partial components with $s \gg l^*$, propagating along the layers with $L \ll l^*$, their analysis is a difficult tech-

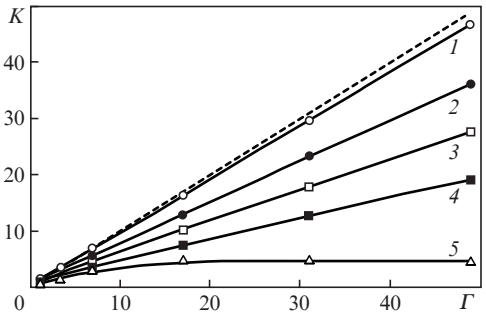

Figure 5. Dependences of K on $\Gamma = \left[\ln\left(n_{\text{eff}}/\sqrt{n_{\text{eff}}^2 - 1}\right)\right]^{-1}$ for the layer with $l^*/L = 2$ and $n_{\text{eff}} = 1.45$, the anisotropy parameter being $g =$ (*1*) 0.1, (*2*) 0.3, (*3*) 0.5, (*4*) 0.7 and (*5*) 0.9. The dashed line corresponds to the case $K = \Gamma$ (isotropic scattering in the layer).

nical problem that requires the use of detectors with a rather wide dynamic range.

4. Conclusions

From the presented results the conclusion follows that the low-coherence interferometric probing of layers in randomly inhomogeneous media is a rather universal approach that allows the analysis of transport characteristics of the probed randomly inhomogeneous medium at a fixed wavelength not only for diffusely scattering media, but also for systems with essential contribution of non-scattered and low-multiplicity-scattered components into the recorded signal. This fact provides a background for essential enhancement of functional capabilities of various approaches in diagnostics and visualisation of randomly inhomogeneous media on the basis of interferometric probing with broadband radiation sources. Of significant interest are further studies of the regime of spatially confined radiation diffusion along optically thin layers of randomly inhomogeneous media, which can be interpreted as a specific manifestation of waveguide propagation of radiation in thin films with large scattering losses.

Acknowledgements. The work was supported by the Russian Foundation for Basic Research (Grant Nos 13-02-00440a and 12-02-31568mol_a).

References

1. Yablonovitch E. *Phys. Rev. Lett*., **58**, 2059 (1987).
2. Ivchenko E.L., Poddubnyi A.N. *Fiz. Tverd. Tela*., **48**, 540 (2006) [*Physics of the Solid State*, **48**, 581 (2006)].
3. Hajian H., Soltani-Vala A., Kalafi M. *Opt. Commun*., **292**, 149 (2013).
4. Vujic D., John S. *Phys. Rev. A*, **72**, 013807 (2005).
5. Fiddy M.A., Schenk J.O., Cao Y. *Opt. Photon. Lett*., **1**, 1 (2008).
6. Veselago V.G. *Usp. Fiz. Nauk*, **92**, 517 (1967) [*Sov. Phys. Usp*., **10**, 509 (1968)].
7. Veselago V.G. *Usp. Fiz. Nauk*, **181**, 1201 (2011) [*Phys. Usp*., **54**, 1161 (2011)].
8. Pendry J.B. *Contemporary Physics* (Princeton, USA: University Princeton Press, 2004) Vol. 45, p. 191.
9. Colodrero S., Calvo M.E., Miguez H., in *Solar Energy*. Ed. by R.D. Rugescu (Croatia : INTECH, 2010) pp 413–432.
10. Van der Molen K.L., Mosk A.P., Lagendijk A. *Opt.Commun*., **278**, 110 (2007).
11. El-Dardiry R.G.S., Lagendijk A. *Appl. Phys. Lett*., **98**, 161106 (2011).
12. Popov A.P., Priezzhev A.V., Lademann J., Myllylä R. *J. Phys. D: Appl. Phys*., **38**, 2564 (2005).
13. Ishimaru A. *Appl. Opt*., **28**, 2210 (1989).
14. Bohren C.F., Huffman D.R. *Absorption and Scattering of Light by Small Particles* (New York: Wiley-Interscience, 1983).
15. Rouston D.D., Poston R.S., Prahl S.A. *J. Biomed. Opt*., **1**, 110 (1996).
16. Leyre S., Durinck G., Giel B.V., Saeys W., Hofkens J., Deconinck G., Hanselaer P. *Opt. Express*, **20**, 17856 (2012).
17. Hennessy R., Lim S.L., Markey M.K., Tunnell J.W. *J. Biomed. Opt*., **18**, 037003 (2013).
18. Wang L., Jacques S. *Appl. Opt*., **34**, 2362 (1995).
19. Zimnyakov D.A., Vilensky M.A. *Opt. Lett*., **31**, 429 (2006).
20. Zimnyakov D.A., Vilenskii M.A. *Opt. Spektrosk*., **104**, 662 (2008) [*Opt. Spectrosc*., **104**, 597 (2008)].
21. Zimnyakov D.A., Isaeva A.A., Isaeva E.A., Ushakova O.V., Zdrazhevskii R.A. *Pis'ma Zh. Tekhn. Fiz*., **38**, 43 (2012) [*Techn. Phys. Lett*., **38**, 925 (2012)].
22. Kienle A., Patterson M.S. *Phys. Med. Biol*., **42**, 1801 (1997).
23. Gurfinkel M., Sevick-Muraca E., Pan T. *J. Biomed. Opt*., **9**, 1336 (2004).
24. Rivas J.G., Dau D.H., Imhof A., Sprik R., Bret B.J.P., Johnson P.M., Hijmans T.W., Lagendijk A. *Opt. Commun*., **220**, 17 (2003).
25. Fercher A.F., Mengedoht K., Werner W. *Opt. Lett*., **13**, 186 (1988).
26. Huang D., Swanson E.A., Lin C.P., Schuman J.P., Stinson W.G., Chang W., Hee M.R., Flotte T., Gregory K., Puliafito C.A., Fujimoto J.F. *Science*, **254**, 1178 (1991).
27. Gelikonov V.M., Gelikonov V.G., Gladkova N.D., Kuranov R.V., Nikulin N.K., Petrova G.A., Pochinko V.V., Pravdenko K.I., Sergeev A.M., Feldshtein F.I., Khanin Ya.I., Shabanov D.V. *Pis'ma Zh. Teor. Eksp. Fiz*., **61**, 149 (1995) [*JETP Lett*., **61**, 158 (1995)].
28. Fercher A.F., Drexler W., Hitzenberger C.K., Lasser T. *Rep. Prog. Phys*., **66**, 239 (2003).
29. Davidson B.R., Barton J.K. *J. Biomed. Opt*., **15**, 016009 (2010).
30. Meemon P., Yao J., Lee K.-S., Thompson K.P., Ponting M., Baer E., Rolland J.P. *Sci. Pep*., **3**, 1709 (2013).
31. Johnson P.M., Imhof A., Bret B.J.P., Rivas J.G., Lagendijk A. *Phys. Rev. E*, **68**, 016604 (2003).
32. Vera M.J., Durian D.J. *Phys. Rev. E*, **53**, 3215 (1996).
33. Soukoulis C.M., Datta S., Economou E.N. *Phys. Rev. B*, **49**, 3800 (1994).
34. Busch K., Soukoulis C.M., Economou E.N. *Phys. Rev. B*, **50**, 93 (1994).
35. Zimnyakov D.A., Pravdin A.B., Kuznetsova L.V., Kochubey V.I., Tuchin V.V., Wang R.K., Ushakova O.V. *J. Opt. Soc. Am. A*, **24**, 711 (2007).
36. http://www.ioffe.ru/SVA/NSM/nk/Oxides/Gif/tio2b.gif.
37. Jacques S.L., Wang L.-H., in *Optical Thermal Response of Laser Irradiated Tissue*. Ed. by A.J. Welch, M.J.C. van Gemert (New York: Plenum Press, 1995) pp 73–100.
38. Zimnyakov D.A., Sinichkin Yu.P., Agafonov D.N., Zakharov P.V. *Waves in Random Media*, **11**, 395 (2001).
39. Henyey L.C., Greenstein J.L. *Astrophys. J.*, **93**, 70 (1941).